90 *Inorg. Chem.* **2011**, *50*, 90–103
DOI: 10.1021/ic1013158

Inorganic Chemistry
Article

Real-Space Indicators for Chemical Bonding. Experimental and Theoretical Electron Density Studies of Four Deltahedral Boranes

Stefan Mebs,[†] Roman Kalinowski,[†] Simon Grabowsky,[†] Diana Förster,[†] Rainer Kickbusch,[†] Eugen Justus,[‡] Wolfgang Morgenroth,[§] Carsten Paulmann,[⊥] Peter Luger,[†] Detlef Gabel,[‡] and Dieter Lentz*[,†]

[†]*Institut für Chemie und Biochemie/Anorganische Chemie, Freie Universität Berlin, Fabeckstrasse 34-36 and 36a, 14195 Berlin, Germany,* [‡]*Institut für Chemie und Biochemie/Fachbereich 2, Universität Bremen, Leobener Strasse, 28359 Bremen, Germany,* [§]*Institut für Geowissenschaften, Facheinheit Mineralogie/Abt. Kristallographie, J. W. Goethe Universität, Altenhöferallee 1, 60438 Frankfurt, Germany, and* [⊥]*Mineralogisch-Petrographisches Institut, Universität Hamburg, Grindelallee 48, 20146 Hamburg, Germany*

Received July 1, 2010

In an approach combining high-resolution X-ray diffraction at low temperatures with density functional theory calculations, two *closo*-borates, $B_{12}H_{12}^{2-}$ (**1**) and $B_{10}H_{10}^{2-}$ (**2**), and two *arachno*-boranes, $B_{10}H_{12}L_2$ [L = amine (**3**) or acetonitrile (**4**)], were analyzed by means of the atoms-in-molecules (AIM) theory and electron localizability indicator (ELI-D). The two-electron three-center (2e3c) bonds of the borane cages are investigated with the focus on real-space indicators for chemical bonding and electron delocalization. In compound **2**, only two of the three expected bond critical points (bcp's) are found. However, a weakly populated ELI-D basin is found for this pair of adjacent B atoms and the delocalization index and the Source contributions are on the same order of magnitude as those for the other pairs. The opposite situation is found in the *arachno*-boranes, where no ELI-D basins are found for two types of B−B pairs, which, in turn, exhibit a bcp. However, again the delocalization index is on the same order of magnitude for this bonding interaction. The results show that an unambiguous real-space criterion for chemical bonding is not given yet for this class of compounds. The *arachno*-boranes carry a special B−B bond, which is the edge of the crown-shaped molecule. This bond is very long and extremely curved inward the B−B−B ring. Nevertheless, the corresponding bond ellipticity is quite small and the ELI-D value at the attractor position of the disynaptic valence basin is remarkably larger than those for all other B−B valence basins. Furthermore, the value of the ED is large in relation to the B−B bond length, so that only this bond type does not follow a linear relationship of the ED value at the bcp versus B−B bond distances, which is found for all other B−B bcp's. The results indicate that both 2e2c and 2e3c bonding play a distinct role in borane chemistry.

Introduction

Because of the electron-deficient nature of the B atom, the complex bonding patterns in boranes cannot be explained by the Lewis electron-pair model.[1] Lipscomb[2] and Wade[3] developed electron-counting rules to explain and predict borane structures. Later, localized bonding models including three-dimensional analogues of Kekulé structures were applied to deltahedral boranes[4] as the idea of three-dimensional aromaticity arose. These models were replaced by the graph theoretical approach of King and Rouvray[5] and the tensor surface harmonic theory of Stone,[6] which approximates the borane deltahedra by spheres. Together with the "six interstitial electron rule" of Jemmis[7] and the classification of the *closo*-borates and carboranes by Williams,[8] the bonding in deltahedral boranes is basically understood in terms of quantum chemistry. All approaches are discussed in detail in a review article of 2001.[9]

However, analysis of the three-dimensional electron density (ED) distribution provides complementary information. The ED is an observable and can be not only calculated but also obtained experimentally by high-resolution X-ray diffraction at low temperatures and subsequent multipole refinement, e.g., based on the Hansen−Coppens formalism.[10] An ED either obtained by calculation or reconstructed from

*To whom correspondence should be addressed. E-mail: lentz@chemie.fu-berlin.de.

(1) Lewis, G. N. *Valence and the Structure of Atoms and Molecules*; The Chemical Catalogue Co.: New York, 1923.
(2) Lipscomb, W. N. *Boron Hydrides*; Benjamin: New York, 1963.
(3) Wade, K. *J. Chem. Soc., Chem. Commun.* **1971**, 792–793.
(4) Dixon, D. A.; Kleier, D. A.; Halgren, T. A.; Hall, J. H.; Lipscomp, W. N. *J. Am. Chem. Soc.* **1977**, *99*, 6226–6237.
(5) King, R. B.; Rouvray, D. H. *J. Am. Chem. Soc.* **1977**, *99*, 7834–7840.
(6) Stone, A. *J. Mol. Phys.* **1980**, *41*, 1339–1354.
(7) Jemmis, E. D. *J. Am. Chem. Soc.* **1982**, *104*, 7017–7020.
(8) Williams, R. E. *Chem. Rev.* **1992**, *92*, 177–207.
(9) King, R. B. *Chem. Rev.* **2001**, *101*, 1119–1152.
(10) Hansen, N. K.; Coppens, P. *Acta Crystallogr., Sect. A* **1978**, *34*, 909–921.

 Published on Web 11/29/2010

multipoles can be analyzed topologically by the atoms-in-molecules (AIM) approach of Bader,[11] which enables a quantitative interpretation of atomic and bonding properties. This approach has been applied to a large number of chemical systems,[12] such as fullerenes[13−16] for which the concept of spherical aromaticity applies as well.[17]

The molecular or crystalline ED of any given assemblage of atoms typically exhibits bond paths (and related bond critical points, bcp's) linking adjacent atoms. In covalent-bonded systems, these bond paths unambiguously correspond to the molecular graph, which intuitively would be drawn by chemists. Moreover, bond paths are found for all types of chemical interactions, including ionic, metallic, and intermolecular hydrogen-bonded and van der Waals bonded systems. Therefore, the existence of a bond path was often mistakenly related to the existence of a chemical bond between the linked atoms. Bader recently commented on that.[18] According to the "orthodox" interpretation, the occurrence of a bond path (and thus a bcp) is a necessary and sufficient condition for two atoms to be *bonded* to each other.[19] In recent years, however, it was demonstrated that this "orthodox" interpretation has its limitations because it does not provide a gradual criterion for chemical bonding, but a yes−no relationship: either there is a bond path or there is none. This was found to be questionable for multicenter bonded systems like supported metal carbonyls[20] and clusters of main-group elements like boranes. Three further points have to be considered in this respect: in experiment, mainly static EDs are topologically interpreted, which by definition excludes the electronic effect of molecular vibration and crystalline libration. These effects, however, could easily lead to the appearance or disappearance of bond paths for bonding scenarios that are close to a catastrophe point. In theory, on the other hand, a sensitivity of the topology against the choice of the computational method was discovered.[21−23] Finally, a bias can be introduced by the nonuniqueness and restrictions of the multipole model itself.[24,25] In answer to these uncertainties, two conceptual progresses were introduced: according to the interpretation of Pendás et al., a bond path actually defines a preferred quantum-mechanical exchange channel between two atoms,[26] an interpretation that relates the ED to energetic contributions of the adjacent atoms. The second progress was the analysis of other descriptors for chemical bonding, such as the electron localization function (ELF),[27,28] the delocalization index $[\delta(x,y)]$,[29,30] the domain-averaged Fermi holes (DAFHs),[31] and others, which provide gradual information about chemical interactions. A recent overview is given by Gatti.[32]

Within this work, four large deltahedral borates and boranes are analyzed: lutidinium dodecahydro-*closo*-dodecaborate(2−) (**1**), 2,2′-bipyridyn-1-ium decahydro-*closo*-decaborate(2−) (**2**), dodecahydro-*arachno*-bis(amine)borane (**3**), and dodecahydro-*arachno*-bis(acetonitrile)borane (**4**). The approach combines experimental ED determination with a broad variety of theoretical calculations. The AIM partitioning scheme is augmented by newer methods such as the source function (SF)[33,34] and the electron localizability indicator (ELI-D).[35] The SF displays the amount of ED provided by each atom to any reference point (rpt), this means also provided by atoms which are not directly connected to the rp. In such way, delocalization effects can be described with absolute numbers. This is also possible with the above-mentioned delocalization index $\delta(x,y)$, introduced by Bader and Stephens.[29,30] The ELI-D is a further development of the above-mentioned ELF.[27,28] ELF and ELI divide the space into regions of localized electron pairs instead of atoms and therefore greatly complement the AIM theory. The partitioning follows the same rules that are used by AIM to separate atoms from each other.[11] Thus, it is space filling and discrete, providing reliable integrated electron numbers of both core shells and (non)bonded valence electrons. Valence basins connecting two core basins are called disynaptic, whereas lone pairs and H atoms exhibit so-called (protonated) monosynaptic valence basins. The disadvantage of the ELF, not to be comparable between different molecules, because the localization is always related to a uniform electron gas of the very same compound, was discarded with the introduction of the ELI-D. The ELF was widely applied to borane compounds in order to understand delocalization effects, [36−40] but quantitative analysis of this class of compounds is rare.[41] Considering borane chemistry, the most prominent feature of localization functions is that regions of high localization

(11) Bader, R. F. W. *Atoms in Molecules. A Quantum Theory*; Cambridge University Press: Oxford U.K., 1991. Bader, R. F. W. In *The Enzyclopedia of Computational Chemistry*; Schleyer, P. von, R., Alinger, N. L., Clark, T., Gasteiger, J., Kollman, P. A., Schaefer, H. F., III, Schreiner, P. R., Eds.; Wiley: Chichester, U.K., 1998.
(12) Koritsánszky, T.; Coppens, P. *Chem. Rev.* **2001**, *101*, 1583–1628.
(13) Irngartinger, H.; Weber, A.; Oeser, T. *Angew. Chem., Int. Ed.* **1999**, *38*, 1279–1281.
(14) Wagner, A.; Flaig, R.; Zobel, D.; Dittrich, B.; Bombicz, P.; Strümpel, M.; Luger, P.; Koritsanzky, T.; Krane, H. G. *J. Phys. Chem. A* **2002**, *106*, 6581–6590.
(15) Hübschle, C. B.; Scheins, S.; Weber, M.; Luger, P.; Wagner, A.; Troyanov, S. I. *Chem.—Eur. J.* **2007**, *13*, 1910–1920.
(16) Chécińska, L.; Troyanov, S. I.; Mebs, S.; Hübschle, C. B.; Luger, P. *Chem. Commun.* **2007**, *39*, 4003–4005.
(17) Chen, Z.; King, R. B. *Chem. Rev.* **2005**, *105*, 3613–3642.
(18) Bader, F. W. R. *J. Phys. Chem. A* **2009**, *113*, 10391–10396.
(19) Bader, R. F. W. *J. Phys. Chem. A* **1998**, *102*, 7314–7323.
(20) Ponec, R.; Gatti, C. *Inorg. Chem.* **2009**, *48*, 11024–11031.
(21) Reinhold, J.; Kluge, O.; Mealli, C. *Inorg. Chem.* **2007**, *46*, 7142–7147.
(22) Henn, J.; Ilge, D.; Leusser, D.; Stalke, D.; Engels, B. *J. Phys. Chem. A* **2004**, *108*, 9442–9452.
(23) Götz, K.; Kaupp, M.; Braunschweig, H.; Stalke, D. *Chem.—Eur. J.* **2009**, *15*, 623–632.
(24) Peres, N.; Boukhris, A.; Souhassou, M.; Gaboille, G.; Lecomte, C. *Acta Crystallogr., Sect. A* **1999**, *55*, 1038–1048.
(25) Volkov, A; Abramov, Y.; Coppens, P.; Gatti, C. *Acta. Crystallogr., Sect. A* **2000**, *56*, 332–339.
(26) Pendás, A. M.; Francisco, E.; Blanco, M. A.; Gatti, C. *Chem.—Eur. J.* **2007**, *12*, 9362–9371.
(27) Becke, A. D.; Edgecombe, K. E. *J. Chem. Phys.* **1990**, *92*, 5397–5403.
(28) Silvi, B.; Savin, A. *Nature* **1994**, *371*, 683–686.
(29) Bader, R. F. W.; Stephens, M. E. *J. Am. Chem. Soc.* **1975**, *97*, 7391–7399.
(30) Fradera, X.; Austen, M. A.; Bader, R. F. W. *J. Phys. Chem.* **1999**, *A103*, 304–314.
(31) Ponec, R. *J. Math. Chem.* **1997**, *21*, 323–333.
(32) Gatti, C. *Z. Kristallogr.* **2005**, 399–457.
(33) Bader, R. F. W.; Gatti, C. *Chem. Phys. Lett.* **1998**, *287*, 233–238.
(34) Gatti, C.; Cargnoni, F.; Bertini, L. *J. Comput. Chem.* **2003**, *24*, 422–436.
(35) Kohout, M. *Int. J. Quantum Chem.* **2004**, *97*, 651–658.
(36) Burkhardt, A.; Wedig, U.; von Schnering, H. G.; Savin, A. *Z. Anorg. Allg. Chem.* **1993**, *619*, 437–441.
(37) Bader, R. F. W.; Johnson, S.; Tang, T.-H.; Popelier, P. L. A. *J. Chem. Phys.* **1996**, *100*, 15398–15415.
(38) Fässler, T. F.; Savin, A. *Chem. Unserer Zeit* **1997**, *31*, 110–120.
(39) Savin, A.; Nesper, R.; Wengert, S.; Fässler, T. F. *Angew. Chem.* **1997**, *109*, 1892–1918.
(40) Binder, H.; Kellner, R.; Vaas, K.; Hein, M.; Baumann, F.; Wanner, M.; Kaim, W.; Wedig, U.; Hönle, W.; von Schnering, H. G.; Groeger, O.; Engelhardt, G. *Z. Anorg. Allg. Chem.* **1999**, *625*, 1638–1646.
(41) Yamaguchi, M.; Ohishi, Y.; Hosoi, S.; Soga, K.; Kimura, K. *J. Phys.: Conf. Ser.* **2009**, *176*, 012027.

have the form of a dual polyhedron of the deltahedral boron cages.

The 2e3c bonds in deltahedral boranes/borates are known to exhibit a charactistic ED distribution that clearly distinguishes them from classical 2e2c bonds. In an early theoretical study on boranes and carboranes,[42] Bader and Legare found the valence density to be delocalized over the B−B−B ring surfaces. This leads to small values of the ED at the bcp's (about 0.8 e $Å^{-3}$) and unusually high values at the ring critical points (rcp's; about 0.7 e $Å^{-3}$). Furthermore, the flat shape of the valence density results in small negative values of the Laplacian $[\nabla^2\rho(\mathbf{r}_{bcp})]$ at the bcp and in substantially large B−B bond ellipticities (ϵ). Another effect of this "smeared alignment" of electrons between the B atoms is that the bond paths are often curved, mostly in the direction of the ring or cage centers (for further computational studies on boranes and borates, see refs 43−47 and references in ref 9). These findings were confirmed later by experimental and theoretical AIM studies on substituted boranes and carboranes.[48−57] Although experimental ED studies of small deltahedral boranes were published recently,[58−60] up to now, no suitable data were available for the large *closo*-borates $B_{12}H_{12}^{2-}$ and $B_{10}H_{10}^{2-}$ and *arachno*-boranes $B_{12}H_{10}L_2$ (L being a Lewis base ligand). In the 1970's, the molecular charge distribution in decaborane(14)[61,62] was analyzed by deformation density maps, but quantitative analysis of the ED distribution could not be performed at that time.

Experiments

Synthesis of the Compounds. Compound **1** was prepared from $Na_2B_{12}H_{12}$ by adding 2.5 equiv of lutidinium chloride to an aqueous solution. The precipitate was filtered off, washed with water, and recrystallized from water. Compounds **2**−**4** were synthesized according to the literature.[63−66]

X-ray Diffraction and Refinement Procedures. High-resolution data of **4** were collected using a Bruker AXS SMART CCD diffractometer (sealed tube, Mo Kα radiation). For **1**−**3**, synchrotron beamlines F1 and D3 at HASYLAB/DESY were used [λ = 0.5166(2) and 0.5600(2) Å, respectively] because of the small volumes and weak scattering power of the crystals. Crystallographic conditions and the results of the multipole refinements[67] are summarized in Table 1. Further details of the data processing are given in the Supporting Information.

For all compounds, anisotropic thermal parameters were calculated for the H atoms using the program *SHADE2*[68] and held fixed during the refinements.[69] The lengths of the X−H bonds, with X being C or N, were elongated to neutron distances;[70] all terminal (bridging) B−H distances were fixed to 1.19 (1.32) Å using the results of neutron diffraction studies,[71] and for the distances obtained by geometry optimization of the title compounds within this work, see below. The H atoms' bond-directed multipoles were refined up to the hexadecapole level in all cases.[72]

For the bridging H atoms in the *arachno*-boranes, local mirror symmetry was applied. In preliminary refinement steps, all chemically equivalent H atoms were mutually constrained. The chemical constraints were revoked in the last refinement step, but the symmetry was retained. The κ and κ' values for the H atoms were changed to 1.13 and 1.29 for protic H atoms, as suggested by Volkov,[73] and 1.10 and 1.10 for hydridic H atoms, according to our own calculations. This procedure has been applied in a recent study on small boranes.[74] All expansion/contraction parameters were refined in an alternating step-by-step procedure with the multipoles.

(42) Bader, R. F. W.; Legare, D. A. *Can. J. Chem.* **1992**, *70*, 657–676.
(43) Takano, K.; Izuho, M.; Hosoya, H. *J. Phys. Chem.* **1992**, *96*, 6962–6969.
(44) Jemmis, E. D.; Subramanian, G.; Srivastava, I. H.; Gadre, S. R. *J. Phys. Chem.* **1994**, *98*, 6445–6451.
(45) Murakhtanov, V. V.; Polyanskaya, T. M.; Volkov, V. V. *J. Struct. Chem.* **1996**, *37*, 652–663.
(46) Sannigrahi, A. B.; Kar, T. *J. Mol. Struct.* **2000**, *496*, 1–17.
(47) Lobayan, R. M.; Bochicchio, R. C.; Torre, A.; Lain, L. *J. Chem. Theory Comput.* **2009**, *5*, 2030–2043.
(48) Antipin, M. Yu.; Poliakov, A. V.; Kapphan, M.; Tsirel'son, V. G.; Ozerov, R. P.; Struchkov, Y. T. *Organomet. Chem. USSR* **1990**, *3*, 421–426.
(49) Antipin, M.; Boese, R.; Bläser, D.; Maulitz, A. *J. Am. Chem. Soc.* **1997**, *119*, 326–333.
(50) Lyssenko, K. A.; Antipin, M. Yu.; Lebedev, V. N. *Inorg. Chem.* **1998**, *37*, 5834–5843.
(51) Glukhov, I. V.; Antipin, M. Yu.; Lyssenko, K. A. *Eur. J. Inorg. Chem.* **2004**, *7*, 1379–1384.
(52) Glukhov, I. V.; Lyssenko, K. A.; Korlyukov, A. A.; Antipin, M. Yu. *Russ. Chem. Bull., Int. Ed.* **2005**, *54*, 547–559.
(53) Lyssenko, K. A.; Golovanov, D. G.; Meshcheryakov, V. I.; Kudinov, A. R.; Antipin, M. Yu. *Russ. Chem. Bull., Int. Ed.* **2005**, *54*, 933–941.
(54) Glukhov, I. V.; Lyssenko, K. A.; Antipin, M. Yu. *Struct. Chem.* **2007**, *18*, 465–469.
(55) Glukhov, I. V.; Lyssenko, K. A.; Korlyukov, A. A.; Antipin, M. Yu. *Faraday Discuss.* **2007**, *135*, 203–215.
(56) Kononova, E. G.; Leites, L. A.; Bukalov, S. S.; Pisareva, I. V.; Chizhevsky, I. T. *J. Mol. Struct.* **2006**, *794*, 148–153.
(57) Kononova, E. G.; Leites, L. A.; Bukalov, S. S.; Pisareva, I. V.; Chizhevsky, I. T.; Kennedy, J. D.; Bould, J. *Eur. J. Inorg. Chem.* **2007**, *31*, 4911–4918.
(58) Förster, D.; Scheins, S.; Luger, P.; Lentz, D.; Preetz, W. *Eur. J. Inorg. Chem.* **2007**, *20*, 3169–3172.
(59) Förster, D.; Hübschle, C. B.; Luger, P.; Hügle, T.; Lentz, D. *Inorg. Chem.* **2008**, *47*, 1874–1876.
(60) Panda, M.; Hofmann, K.; Prosenc, M. H.; Albert, B. *Dalton Trans.* **2008**, 3956–3958.
(61) Brill, R.; Dietrich, H.; Dierks, H. *Acta Crystallogr., Sect. B* **1971**, *27*, 2003–2018.
(62) Dietrich, H.; Scheringer, C. *Acta Crystallogr., Sect. B* **1978**, *34*, 54–63.
(63) Hawthorne, M. F.; Pilling, R. L.; Grimes, R. N. *J. Am. Chem. Soc.* **1967**, *89*, 1067–1074.
(64) Muetterties, E. L.; Balthis, J. H.; Chia, Y. T.; Knoth, W. H.; Miller, H. C. *Inorg. Chem.* **1964**, *3*, 444–451.
(65) Williams, J.; Williams, R. L.; Wright, J. C. *J. Chem. Soc.* **1963**, 5816–5824.
(66) Beall, H. *Inorg. Chem.* **1972**, *11*, 637.
(67) Volkov, A.; Macchi, P.; Farrugia, L. J.; Gatti, C.; Mallinson, P.; Richter, T.; Koritsanszky, T. *XD2006, a computer program for multipole refinement, topological analysis of charge densities and evaluation of intermolecular energies from experimental or theoretical structure factors, User Manual*, 2006.
(68) Madsen, A. Ø.; Sørensen, H. O.; Flensburg, C.; Stewart, R. F.; Larsen, S. *Acta Crystallogr., Sect. A* **2004**, *60*, 550–561.
(69) Because H atoms connected to borane are not in the SHADE dictionary yet, the default internal mean-square displacements of 0.005, 0.020, and 0.020 $Å^2$ were assigned to them. For validation of the used model, which pushes the limits, standard refinements were repeated for compound **3** with isotropic H atoms and multipoles refined up to the quadrupole level for H atoms. Bond topological properties were obtained for this model and included in the Supporting Information, Table S10. As expected, all numbers show differences, but it is not possible to decide which of the results is to be preferred. Because the trends are the same for both refinements of compound **3**, it was decided not to pursue this question in more detail.
(70) Wilson, A. J. C. *International Tables of Crystallography*; Kluwer Academic Publishers: Boston, 1992; Vol. *C*.
(71) Tippe, A.; Hamilton, W. C. *Inorg. Chem.* **1969**, *8*, 464–470.
(72) For EDs reconstructed from multipole refinement of theoretical structure factors,[79,78] we have observed that properties derived from the ED, such as the electrostatic potential, are closer to the results directly obtained from the wave function when the H atoms are also expanded to the hexadecapole level (only bond directed multipoles are refined). This approach is already applied in the Invariom formalism, which is used for application of the theoretical multipole density to experimental data of lower resolution and/or macromolecules. See: Dittrich, B.; Koritsánszky, T.; Luger, P. *Angew. Chem., Int. Ed.* **2004**, *43*, 2718–2721.
(73) Volkov, A.; Abramov, Y.; Coppens, P. *Acta Crystallogr., Sect. A* **2001**, *57*, 272–282.
(74) Mebs, S.; Grabowsky, S.; Förster, D.; Kickbusch, R.; Hartl, M.; Daemen, L. L.; Morgenroth, W.; Luger, P.; Paulus, B.; Lentz, D. *J. Phys. Chem. A* **2010**, *114*, 10185–10196.

Table 1. Crystallographic Data and Experimental Conditions

compound	1,3-lutidinium dodecaborate	2,2-bis(pyridilium) dodecaborate	bis(amine) dodecaborate	bis(acetonitrile) dodecaborate
Wade cluster type	closo	closo	arachno	arachno
label	**1**	**2**	**3**	**4**
empirical formula	$[B_{12}H_{12}^{2-}][(C_7H_{10}N^+)_2]$	$[B_{10}H_{10}^{2-}][(C_{10}H_9N_2^+)_2]$	$B_{10}H_{12}(NH_3)_2$	$B_{10}H_{12}(NCCH_3)_2$
formula weight [g mol^{-1}]	358.14	450.58	154.26	202.30
cryst syst	monoclinic	triclinic	orthorhombic	monoclinic
space group	$P2_1/n$ (No. 14)	$P\bar{1}$ (No. 2)	*Pnma* (No. 62)	$C2/c$ (No. 15)
Z	2	2	4	4
temp [K]	100(2)	9(2)	9(2)	95(2)
a [Å]	9.920(2)	9.232(2)	17.863(4)	15.187(3)
b [Å]	9.190(2)	9.437(2)	7.316(2)	11.127(2)
c [Å]	11.841(2)	14.613(3)	7.177(1)	7.762(1)
α [deg]	90.00	86.66(3)	90.00	90.00
β [deg]	95.88(3)	83.88(3)	90.00	112.66(1)
γ [deg]	90.00	72.83(3)	90.00	90.00
V [Å^3]	1073.8(4)	1209.0(5)	937.9(3)	1210.3(4)
calcd density [g cm^{-3}]	1.1076(4)	1.2377(5)	1.0925(3)	1.1103(4)
$F(000)$	380.0	472.0	328.0	424.0
crystal size [mm^3]	0.3 × 0.25 × 0.2	0.2 × 0.2 × 0.15	0.3 × 0.2 × 0.15	0.5 × 0.35 × 0.35
λ [Å]	0.5600(2) (synchr.)	0.5166(2) (synchr.)	0.5166(2) (synchr.)	0.710 73
sin θ/λ_{max} [Å^{-1}]	1.16	1.02	1.00	1.15
colld reflns	133297	194515	62260	44091
symmetry indep	13935	19381	4131	7423
completeness [%]	99.3	90.1	99.8	96.3
redundancy	9.6	10.0	15.1	5.9
R_{int}	9.54	7.16	15.24	2.80
μ [mm^{-1}]	0.02	0.05	0.04	0.05
R1 (spherical)	4.67	3.71	3.57	3.57
$N_{ref}/N_{var.}$ (multipole)	29.2	15.9	11.5	24.5
$R_w(F^2)$ (multipole)[a]	8.34	4.83	6.08	2.98
$R(F)$ (multipole)	3.26	2.13	2.53	1.71
$R_{all}(F)$ (multipole)	6.89	3.92	5.60	4.53
included ($I > 2\sigma$)	8030	13527	2448	5292
GOF	0.594	0.574	0.451	0.604
$\Delta\rho_{min}$, $\Delta\rho_{max}$ [e Å^{-3}]	−0.250, 0.260[b]	−0.207, 0.401	−0.191, 0.262	−0.153, 0.112

[a] Refinement against F^2. [b] A singular positive residual density of 0.678 e Å^{-3} is located between the molecules.

B and N atoms were refined up to the hexadecapole level as well. For B atoms connected to five other B atoms, 5-fold symmetry was approximated by a combination of *m* symmetry and chemically constraints for all equal atoms. For the apical B atoms in **2** (see Figure 1), 4-fold symmetry was applied. For all B atoms in the *arachno*-boranes, except for the four being connected to the bridging H atoms, mirror symmetry was applied. The latter ones were refined without symmetry restrictions. In all four compounds, chemically identical B atoms were mutually constrained.

Theoretical Calculations

Several ED-derived properties like the delocalization index[29,30] [$\delta(x,y)$] and the integrated amount of electrons within the zero flux surface (zfs; $\oint_{x\cap y}$) cannot (yet) be derived from experimental data. Moreover, the ELI-D can only be calculated from the wave function. Hence, a variety of theoretical calculations were performed in order to supplement experimental findings:

Model *gas* corresponds to the unrestricted geometry optimizations (*Gaussian03*[75]) of the isolated title compounds at the B3LYP/6-311+g(2d,2p) level of theory. The wave functions were analyzed with *AIM2000*,[76] *DGRID-4.4*,[77] and *TONTO*[78] to obtain all bond and atomic properties presented in this study. Details are given in the Supporting Information.

Moreover, the geometries obtained by multipole refinement were used for single-point calculations at periodic boundary conditions using the program *Crystal06*,[79] model *cry*.[80] With the program *Properties06* of the *Crystal06* program package, theoretical structure factors were calculated using the *hkl* sets of the four X-ray diffraction experiments. In subsequent XD refinements using the same local coordinate systems and symmetry restrictions as those in the experimental cases, theoretical ED models (*cry*), including intermolecular interactions, were obtained. Although calculations at the experimental geometry do not refer to the minimum-energy crystal structure, they were chosen in order to retain comparability to the experimental results.

The experimental results will be denoted as model *exp*.

Results and Discussion

Structures. Figure 1 displays the structures of the title compounds as ORTEP plots[81] including the labeling

(75) Frisch, M. J.; et al. *Gaussian03*, revision D.01; Gaussian, Inc.: Wallingford, CT, 2004.

(76) Biegler-König, F.; Schönbohm, J.; Bayles, D. AIM2000—A Program to Analyse and Visualize Atoms in Molecules. *J. Comput. Chem.* **2001**, *22*, 545−559.

(77) Kohout, M. *DGrid and Basin*, version 4.4; Max-Planck-Institut für Chemische Physik fester Stoffe: Dresden, Germany, 2009.

(78) Jayatilaka, D.; Grimwood, D. J. *TONTO: A Fortran Based Object-Oriented System for Quantum Chemistry and Crystallography, User Manual*: The University of Western Australia, Perth, Australia, 2003.

(79) Dovesi, R.; Saunders, V. R.; Roetti, C.; Orlando, R.; Zicovich-Wilson, C. M.; Pascale, F.; Civalleri, B.; Doll, K.; Harrison, N.; Bush, I.; D'Arko, P.; Llunell, M. *Crystal06, User's Manual*, version 1.0.2; University of Torino: Torino, Italy, 2006.

(80) The basis sets were chosen from the Crystal06 Basis Sets Library to balance each other. They were at least of polarized double-ζ quality: oxygen, 6-31d1; carbon, 6-31d1G; hydrogen, 3-1p1G (Gatti, C.; Saunders, V. R.; Roetti, C. *J. Chem. Phys.* **1994**, *101*, 10686−10696); nitrogen, 6-21G* (Dovesi, R.; Causá, M.; Orlando, R.; Roetti, C. *J. Chem. Phys.* **1990**, *92*, 7402−7411); boron, 6-21G* (Orlando, R.; Dovesi, R.; Roetti, C. *J. Phys.: Condens. Matter* **1990**, *2*(38), 7769−7789).

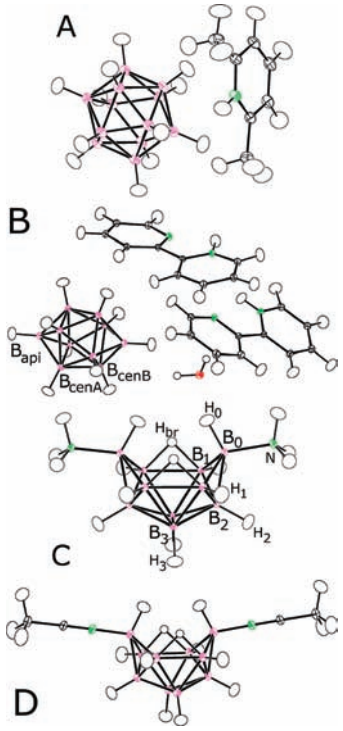

Figure 1. ORTEP plots of the title compounds obtained by high-resolution X-ray diffraction at low temperatures. In **1**, a center of inversion lies at the center of the $B_{12}H_{11}^{2-}$ cage; in **3**, a mirror plane lies along the long molecular axis, resulting in special positions for the N atoms, four B atoms, and six H atoms; in **4**, the molecule is constructed by a 2-fold axis, which goes through the B_3-B_3 axis and the center of the cage. The labeling of **4** corresponds to that of **3**. In **1**, all B atoms are simply labeled as B in the following tables and figures.

scheme. In compound **2**, the capping B atoms are denoted as B_{api}, whereas the B atoms within the square antiprisms are labeled as B_{cen}. Bonds connecting a B atom of one square with a B atom of the second square are denoted as $B_{cenA}-B_{cenB}$. In the *arachno*-boranes (**3** and **4**), the situation is more complex. Four different B atoms exist in the cages. The two equivalent B atoms involved in the dative bonds are labeled B_0, the four equivalent B atoms bonded to the bridging H atom are labeled B_1, the two B atoms bonded to B_0 and B_1 are labeled B_2, and the two central B atoms, which are bonded to each other, are labeled B_3.

In the Supporting Information, tables including averaged B−B bond lengths and B−B−B (B−B−H) angles are given for compounds **1** and **2**. For **3** and **4**, complete lists of the corresponding lengths and angles are given. In compound **1**, the averaged bond B−B−B angles are found to be the ideal icosahedral angles of 60° and 108°; thus, when a slightly larger spread in the B−B−H angles is disregarded, the icosahedral symmetry is retained.[82]

In compound **2**, two types of B−B−B triangles exist, $B_{cen}-B_{api}-B_{cen}$ and $B_{cenA}-B_{cenB}-B_{cenA}$ with corresponding bond angles of 65.3(3)° and 60.8(2)°.[83]

The *arachno*-boranes carry two types of *m*-symmetrical B−B−B triangles ($B_3-B_2-B_3$ and $B_1-B_3-B_1$; central atoms exhibit angles of 62−63°) and two unsymmetrical B−B−B triangles ($B_0-B_2-B_1$ and $B_1-B_2-B_3$; central atoms exhibit angles of about 64° and 61°) each. For the latter unsymmetrical triangle ($B_1-B_2-B_3$), the remaining averaged angles are 59.8(2)° and 59.5(1)°. Thus, the asymmetry is weak, whereas for the $B_0-B_2-B_1$ triangle, the remaining averaged angles are 58.3(1)° and 57.4(2)°. This asymmetry is also found in the bond topological properties; see the next section.[84]

The 2e3c Bond. Electron Distribution in the B−B−B and B−H−B Ring Planes. In Figures 2 and 3, five B−B−B rings of compounds **1**, **2**, and **4** and the $B-H_{bridge}-B$ ring of the *arachno*-borane **4** are presented in terms of experimental static deformation densities (sdd), corresponding Laplacian $[\nabla^2\rho(\mathbf{r}_{bcp})]$ maps, and gradient vector field (gvf) plots.

Parts A−C of Figure 2 display the results for **1**. The sdd shows a remarkably low amount of aspherical density, which is distributed symmetrically over the ring plane instead of being accumulated between the B atoms, as would be expected for a classical 2e2c bond scenario. The same is found in the corresponding Laplacian: nevertheless, weak valence shell charge concentrations (vscc's) are found on the B−B axes, a characteristic feature of covalent bonds. Because of the icosahedral molecular symmetry and the constraints applied in the modeling of the aspherical densities, both maps are symmetrical. In the gvf, bcp's are found in the midpoints of all 30 B−B axes of the icosahedron and rcp's are found in all 20 B−B−B ring centers. Finally, a cage critical point (ccp) is found in the center of the boron cage.

Parts D−I of Figure 2 display the corresponding ED distributions for compound **2**. Parts D and G of Figure 2 reveal that no bond path and thus no vscc's are exhibited between the B_{cen} atoms within the same square plane of the antiprism, whereas they are found on the $B_{cen}-B_{api}$ axes (Figure 2E,F) as well as on the $B_{cenA}-B_{cenB}$ axes (Figure 2H,I). Topologically, a folded four-membered ring ($B_{cenA}-B_{api}-B_{cenA}-B_{cenB}$) is formed, with the rcp located almost in the midpoint of the triangle formed by the central B atoms (Figure 2I). Moreover, the molecular graph shows some strain in the $B_{cenA}-B_{cenB}$ bonds.

In ref 57, the $B_{11}H_{11}^{2-}$ dianion was investigated. In the AIM analysis, a pair of B atoms did not exhibit an expected bond path as well. Thus, it was stated that "... the formally closed eleven-vertex polyhedra [...] are not formed by triangular faces only, and therefore do not

(81) Burnett, M. N.; Johnson, C. K. ORTEP-III, Oak Ridge Thermal Ellipsoid Plotting Program for Crystal Structure Illustrations. Report ORNL-6895; Oak Ridge National Laboratory: Tennessee, TN, **1996**.

(82) Experimental B−B bonds vary from 1.780 to 1.791 Å, with an average of 1.785(3) Å. The following min/average (sd)/max values are obtained for the dihedral and acute B−B−B angles and the B−B−H angles: 107.6°/108.0(2)°/108.4°, 59.7°/60.0(1)°/60.3°, and 117.8°/121.7(1.9)°/125.9°. For the gas-phase optimization (*gas*), the following bond lengths were obtained: d(B−B) = 1.783 Å; d(B−H) = 1.200 Å.

(83) Experimental bond lengths are as follows: $B_{cen}-B_{api}/B_{cenA}-B_{cenB}/B_{cenA}-B_{cenA}$ 1.701(3)/1.813(6)/1.835(6) Å. The average of all bond lengths is 1.783(60) Å and thus is very close to the value found in compound **1**. For model *gas*, the following values were obtained: $d(B_{cen}-B_{api})$ = 1.699 Å; $d(B_{cenA}-B_{cenB})$=1.818 Å; $d(B_{cenA}-B_{cenA})$=1.838 Å; $d(B_{api}-H_{api})$=1.200 Å; $d(B_{cen}-H_{cen})$ = 1.204 Å; $\angle(B_{cen}-B_{api}-B_{cen})$ = 65.48°; $\angle(B_{cenA}-B_{cenB}-B_{cenA})$ = 60.73°.

(84) B−B bond distances vary from about 1.73 to 1.87 Å, with an average of 1.796(48) Å weighted over the appearance of identical bonds, which is slightly larger than the value of 1.785(3) Å found for the B icosahedron. For model *gas*, the following values were obtained: $d(B_0-B_1)$ = 1.751 Å; $d(B_0-B_2)$ = 1.733 Å; $d(B_1-B_1)$ = 1.871 Å; $d(B_1-B_3)$ = 1.781 Å; $d(B_2-B_3)$ = 1.750 Å; $d(B_3-B_3)$ = 1.833 Å; $d(B_0-H)$ = 1.189 Å; $d(B_1-H)$ = 1.190 Å; $d(B_2-H)$ = 1.195 Å; $d(B_3-H)$ = 1.184 Å; $d(B_1-H_{bridge})$ = 1.317 Å. All B−B−B angles are very close to the experimental results.

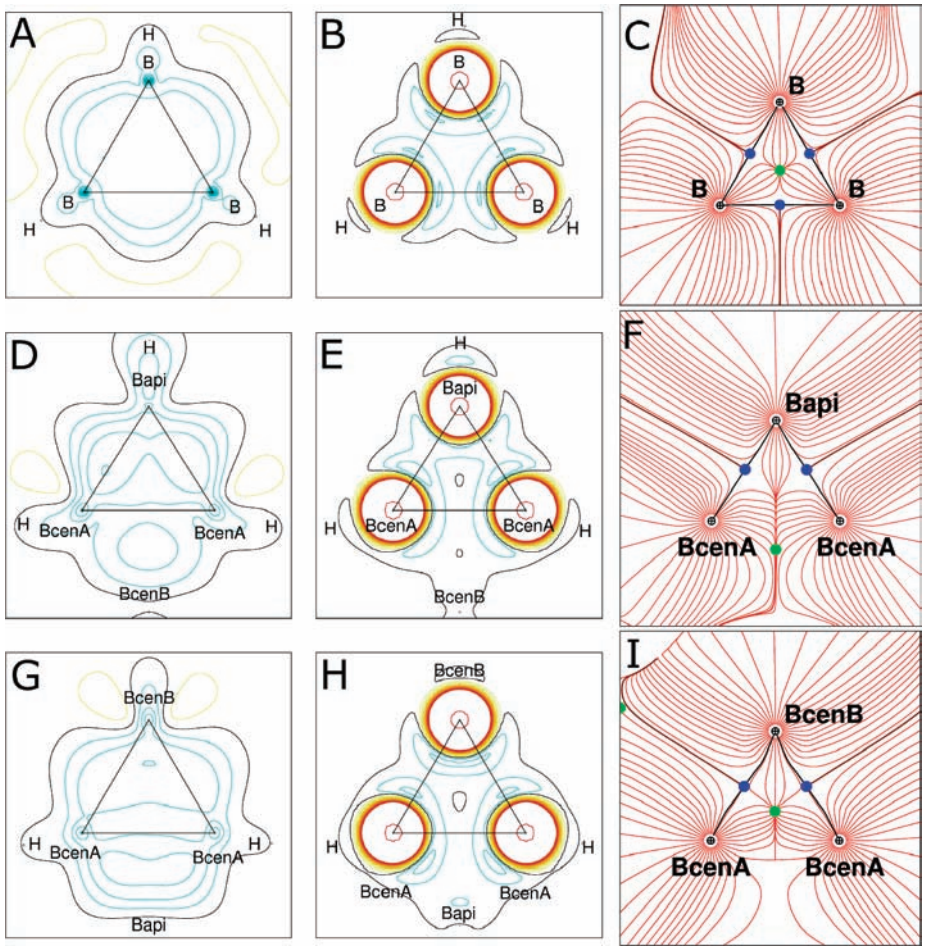

Figure 2. (A−C) Experimental sdd, Laplacian (L), and gvf maps of **1**, (D−F) corresponding maps of the $B_{cen}-B_{api}-B_{cen}$ triangle in **2**, and (G−I) corresponding maps of the $B_{cenA}-B_{cenB}-B_{cenA}$ triangle in **2**. For sdd, contour lines are 0.05 e Å^{-3} and blue lines refer to positive values, black is zero, and yellow is negative. For L, contour lines are 2.5 e Å^{-5} and blue lines refer to negative values, black is zero, and yellow/red is positive. For gvf, gradient paths are red, zfs's are black, blue dots are bcp's, and green dots are rcp's.

have genuine *closo* structures, in spite of having (2n+2) skeletal bonding electrons." This is also true for compound **2**, for which *no closed deltahedron is found at all* in terms of AIM topology.

As discussed in the Structures section, the *arachno*-boranes contain four different B−B−B triangles and one B−H−B triangle. Parts A−I of Figure 3 display the ED properties of $B_0-B_1-B_2$ (unsymmetrical), $B_1-B_3-B_1$ (symmetrical), and $B_1-H_{bridge}-B_1$ (symmetrical) of compound **4**. The corresponding maps for compound **3** are given in the Supporting Information. The remaining rings ($B_1-B_2-B_3$ and $B_3-B_2-B_3$) are not shown because they are comparable to the "ideal" case of compound **1**.

In the three general structure types icosahedron, bicapped square antiprism, and *arachno*-cage, the terminal $B_0-B_1-B_2$ ring (Figure 3A−C) is the most unsymmetrical ring, which has the longest B−B distance (B_0-B_1) of about 1.86 Å and an even longer bond path (about 1.91 Å). The sdd of this plane shows the general features of B−B−B triangles, but in addition, a curved charge accumulation close to the B_0-B_1 axis appears inward the ring, which is also visible in the Laplacian and gvf. Nevertheless, the rcp is still located close to the midpoint of the triangle spanned by the three B−B axes instead of being shifted toward the midpoint of the three bcp's. As a consequence, the bcp of the long B_0-B_1 bond comes very close to the rcp, thus being close to a catastrophic scenario, where bcp and rcp melt together and the B_0-B_1 bond vanishes.

The symmetrical $B_1-B_3-B_1$ and $B_1-H_{bridge}-B_1$ triangles (Figure 3D−F,G−I) are connected to each other by the B_1-B_1 axis. Both show the general features that are found in the triangles of **2**; that is, the charge is depleted in the B_1-B_1 axis, and no bcp is found between these atoms. This is known from the literature.[42,59] The gvf reveals that the rcp of this folded four-membered ring $B_1-H_{bridge}-B_1-B_3$ is located close to the midpoint of the B−B−B triangle. As for the terminal B_0-B_1 bond, the bond path of the terminal B_1-H_{bridge} bond is curved inward the B−H−B triangle, so that all cusps of the crown-shaped *arachno*-boranes show this feature.

The degree of delocalization depends on the chemical environment of the bond (i.e., embedded in a cage or located at the edges of the molecule) and the molecular symmetry. As a consequence, not eight but six rings are distinguishable within the three general structure types in terms of AIM topology.

Properties of the "Missing" bcp's. In order to reveal the reason why no bcp is exhibited between certain pairs of B atoms, the experimental ED and derived properties such as the gradient of the ED, the Laplacian, and the local source (LS) were evaluated along a B−B axis in **1**, along a

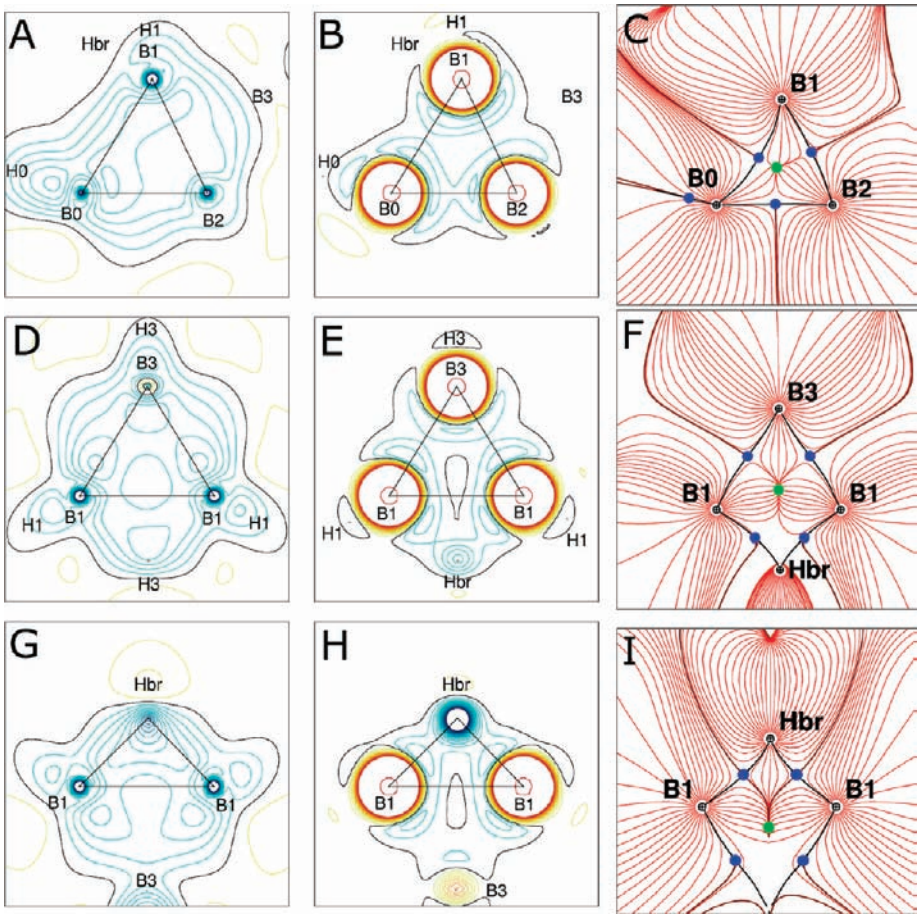

Figure 3. (A−C) Experimental sdd, Laplacian, and gvf maps of the $B_0-B_1-B_2$ ring in **4**, (D−F) corresponding maps of the $B_1-B_3-B_1$ ring; and (G−I) corresponding maps of the $B_1-H_{bridge}-B_1$ ring. Contour lines are 0.05 e Å^{-3} for the deformation densities and 2.5 e Å^{-5} for the Laplacians. For the color scheme, see Figure 2.

$B_{cenA}-B_{cenA}$ axis in **2**, and along a B_1-B_1 axis in **3**; see Figure 4A−C. The corresponding axes, which are perpendicular to the B−B axes, are analyzed in the same way; see Figures 4D−F and S6 in the Supporting Information. Theoretical results for **2** are given in Figure S7 in the Supporting Information.

Interestingly, for all three B−B axes (Figure 4A−C), all given properties qualitatively behave similarly. Moreover, the value of the ED is almost the same at the midpoint of the three B−B axes (which is the reference point, rp). Because of the inwardly curved bond path, the bcp is not located at the rp of the B−B axis in **1**. For perpendicular line plots starting inside the cages (e.g., ccp or center of square; see Figure S6A−C in the Supporting Information), all properties again show a comparable progression of the given properties.

Fundamental differences, however, are found upon analysis of the line plots perpendicular to the B−B axis, which go across the B−B−B or B−H−B ring planes, starting from the adjacent B or H atom, which is not connected to the B−B axis; see Figures 4D−F and S6D−F in the Supporting Information. In compound **1**, a local maximum of the ED is found (see Figures 4D and S6D in the Supporting Information), resulting in a bcp close to the rp. Although the corresponding line plots of **2** (Figures 4E and S6E in the Supporting Information) show some similarities to those of **1**, the gradient never vanishes; thus, no bcp is exhibited. Much larger differences to **1** are found for the corresponding line plots of **3**; see Figures 4F and S6F in the Supporting Information. The different character of the $B_{cenA}-B_{cenA}$ rp and the B_1-B_1 rp is also confirmed by the three principal curvatures of the ED. At the $B_{cenA}-B_{cenA}$ rp, two curvatures are negative, which is characteristic for a bcp, whereas the B_1-B_1 rp only has one negative curvature, which is characteristic for a rcp. One may state that the $B_{cenA}-B_{cenA}$ pair still is quite close to a catastrophic scenario in which a new bcp will be generated. B_1-B_1, however, seems to be far away from such a scenario. Obviously, the line plots provide further information about the charge distribution, which cannot be obtained by the two-dimensional maps of Figures 2 and 3. These results are confirmed by integrated bond properties; see below.

The progression of the properties ED and gradient of the ED and Laplacian through the molecules reveal that the charge is depleted at the ccp's and that spherical ring currents are not reflected in the ED distribution. The corresponding plots are given in the Supporting Information (Figure S8).

In the following paragraphs, the bonding patterns are quantified by a variety of topological and integrated bond descriptors obtained from experiments and calculations.

Bond Topology. Table 2 displays the common bond topological parameters for the nine different types of B−B bcp's found in the title compounds. Because B−B bonds are often curved, the geometrical distances (R_{xy}) as

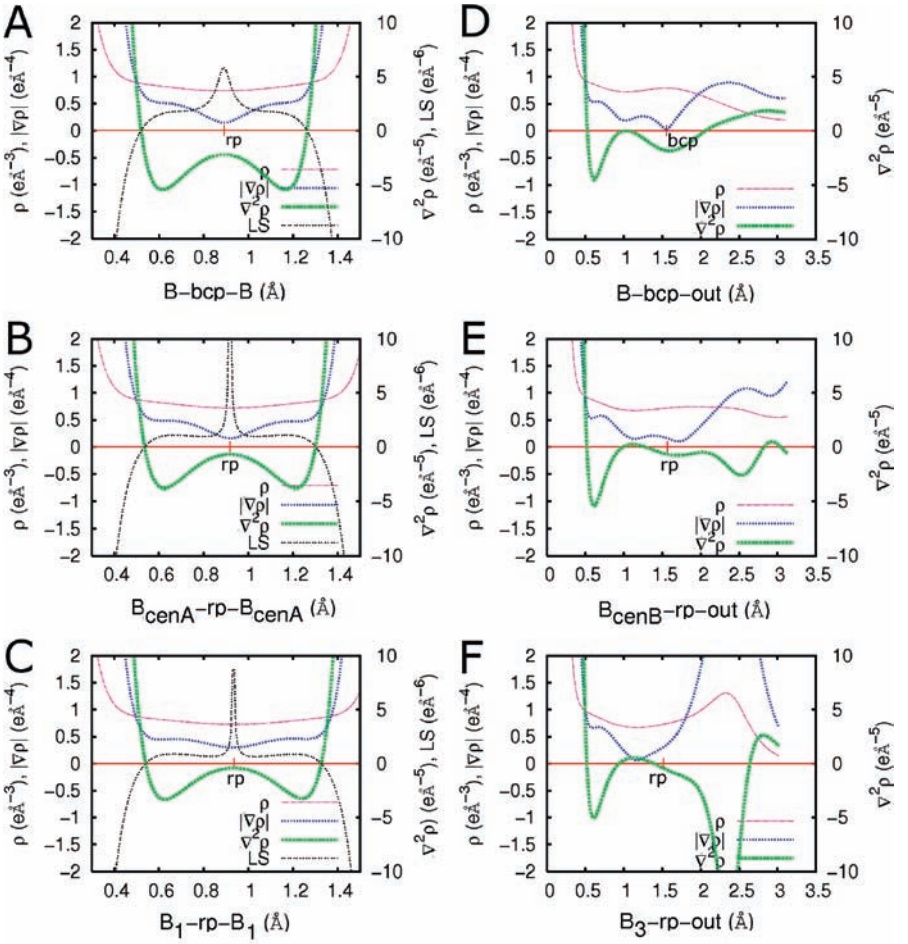

Figure 4. (A−C) Experimental ED, gradient of the ED, Laplacian, and LS plots of a B−B axis in **1**, along the B_{cenA}−B_{cenA} axis in **2**, and along the B_1−B_1 axis in **3** and (D−F) corresponding plots (without LS) along perpendicular axes across B−B−B triangles: (D) B−B−B; (E) B_{cenA}−B_{cenB}−B_{cenA}; (F) B_1−B_3−B_1. "bcp" is the bond critical point, "rp" is the reference point, which is the midpoint of the two B atoms for the calculation of the LS, and "out" means a point outside the molecules, which is the end point of the line.

well as the lengths of the bond paths (R_{bp}) are given. Finally, the distances of the positions of the bcp's perpendicular to the B−B axes (Δ_{bcp}) are listed. The latter two parameters allow one to quantify the strain in the B−B bonds. All results in Table 2 are obtained by multipole refinements of experimental and theoretical structure factors, respectively.[85] Because the terminal B−H bonds are clearly covalent, only one example of a B−H_{term} bond is given (no. 11) together with the more interesting bridging B−H_{bridge} bond of the *arachno*-boranes (no. 10). Because of the large amount of data included in this study, all chemically identical bonds were averaged because they showed no significant differences. The number of contributors for each value is given in the last row (av.). Complete lists of topological parameters for all individual bonds are given in the Supporting Information.

It is apparent that the agreement between the different models (*exp*, *cry*, and *gas*) is good, which means, on the other hand, that any electronic effects of crystallization are only weakly reflected in the topology. The same is true for the electronic differences between the two *arachno*-boranes. These two questions (charge transfer via dihydrogen contacts and via the dative N−B bond) will be investigated in a later publication.

For the B−B bonds, $\rho(\mathbf{r}_{bcp})$ varies from 0.73 to 0.89 e Å^{-3} for bond distances of 1.70−1.87 Å. This is in accordance with the results of previous theoretical studies.[42,57,58] The relation of d_1 to d_2 is quite close to one for all cases because the chemical environments are more or less similar for all B atoms except B_0. In the B−H bonds, the bcp is located closer to the B atom because of the higher electronegativity of the hydridic H atoms.

Disregarding the two outliers of the bonds B_0−B_2 and B_3−B_3 (model **3**-*exp*), ϵ varies from 1 to 6, which is significantly larger than what is found for localized covalent bonds; see, for example, the results of the terminal B−H bonds (no. 11).[86] The ellipticity of the B−B bond in **1** is significantly larger than that of the two different B−B bonds in **2**, which is in accordance with the assumption of a higher degree of electron delocalization in the molecule with higher symmetry. In the *arachno*-boranes, the situation is more complex. Three bonds (nos. 4, 6, and 9) show

(85) For compound **4**, the transformation of the wave-function file from the gas-phase structure into a *hkl* set failed, so that this model is not represented here.

(86) Interestingly, ϵ varies only a little between the models (*exp*, *cry*, and *gas*) for the same bonds, although this parameter is known to be quite sensitive because two curvatures of the ED affect it.

Table 2. Averaged Topological Bond Descriptors of the B−B and B−H Bonds[a]

no.	model	type	$\rho(\mathbf{r}_{bcp})$ [e Å^{-3}]	$\nabla^2\rho(\mathbf{r}_{bcp})$ [e Å^{-5}]	d_1 [Å]	d_2 [Å]	ϵ	R_{xy} [Å]	R_{bp} [Å]	Δ_{bcp} [Å]	av.
1	**1**-*exp*	B−B	0.79(1)	−1.9(1)	0.892	0.893	2.80	1.785	1.787	0.024	15
	1-*cry*		0.79	−2.1	0.892	0.893	3.00	1.785	1.787	0.019	15
	1-*gas*		0.78	−1.6	0.892	0.892	2.40	1.783	1.784	0.023	
2	**2**-*exp*	$B_{cen}-B_{api}$	0.89(1)	−3.2(1)	0.873	0.829	1.36	1.701	1.704	0.018	8
	2-*cry*		0.89	−3.2	0.875	0.827	1.05	1.701	1.703	0.001	8
	2-*gas*		0.89	−2.5	0.865	0.835	1.17	1.699	1.700	0.018	
3	**2**-*exp*	$B_{cenA}-B_{cenB}$	0.77(1)	−1.9(1)	0.907	0.907	1.73	1.813	1.828	0.035	8
	2-*cry*		0.74	−2.0	0.906	0.906	1.83	1.813	1.824	0.012	8
	2-*gas*		0.74	−1.3	0.910	0.910	1.53	1.818	1.831	0.040	
4	**3**-*exp*	B_0-B_2	0.83(1)	−1.4(1)	0.917	0.817	10.32	1.732(1)	1.739	0.043	2
	4-*exp*		0.86(1)	−2.5(1)	0.880	0.871	2.26	1.749(1)	1.754	0.049	1
	3-*cry*		0.84	−2.7	0.895	0.840	3.45	1.732	1.737	0.056	2
	4-*cry*		0.80	−2.2	0.921	0.831	3.73	1.749	1.753	0.047	1
	3-*gas*		0.82	−1.9	0.889	0.847	3.21	1.733	1.738	0.051	
5	**3**-*exp*	B_0-B_1	0.81(1)	−2.6(1)	0.957	0.943	2.47	1.861(1)	1.919	0.190	2
	4-*exp*		0.79(1)	−2.0(1)	0.959	0.939	2.02	1.865(1)	1.911	0.175	2
	3-*cry*		0.80	−2.6	0.932	0.957	1.98	1.861	1.904	0.164	2
	4-*cry*		0.78	−2.5	0.954	0.941	1.90	1.865	1.909	0.167	2
	3-*gas*		0.77	−1.9	0.951	0.930	1.63	1.853	1.890	0.159	
6	**3**-*exp*	B_2-B_1	0.86(1)	−2.6(1)	0.901	0.858	3.26	1.755(1)	1.762	0.057	2
	4-*exp*		0.82(1)	−1.2(1)	0.853	0.918	4.64	1.763(1)	1.779	0.081	2
	3-*cry*		0.81	−1.9	0.840	0.919	6.23	1.755	1.764	0.056	2
	4-*cry*		0.81	−2.0	0.880	0.887	4.41	1.763	1.773	0.051	2
	3-*gas*		0.80	−1.4	0.880	0.874	3.96	1.751	1.758	0.044	
7	**3**-*exp*	B_2-B_3	0.84(1)	−2.5(1)	0.871	0.892	2.12	1.761(1)	1.768	0.028	2
	4-*exp*		0.84(1)	−1.9(1)	0.923	0.844	2.32	1.765(1)	1.768	0.038	2
	3-*cry*		0.82	−2.5	0.907	0.860	2.55	1.761	1.775	0.065	2
	4-*cry*		0.82	−2.4	0.902	0.866	2.78	1.765	1.771	0.050	2
	3-*gas*		0.82	−2.0	0.906	0.846	2.05	1.750	1.756	0.043	
8	**3**-*exp*	B_1-B_3	0.83(1)	−1.9(1)	0.895	0.892	1.73	1.777(1)	1.794	0.094	2
	4-*exp*		0.84(1)	−2.1(1)	0.929	0.860	1.89	1.785(1)	1.794	0.059	2
	3-*cry*		0.83	−2.6	0.898	0.884	1.84	1.777	1.787	0.073	2
	4-*cry*		0.82	−2.5	0.907	0.883	1.94	1.785	1.793	0.069	2
	3-*gas*		0.80	−1.8	0.903	0.884	1.61	1.781	1.790	0.071	
9	**3**-*exp*	B_3-B_3	0.73(2)	−0.5(1)	0.913	0.913	9.50	1.826(1)	1.828	0.011	1
	4-*exp*		0.78(1)	−1.4(1)	0.915	0.915	3.00	1.825(1)	1.833	0.075	1
	3-*cry*		0.75	−1.5	0.914	0.914	3.90	1.826	1.828	0.021	1
	4-*cry*		0.76	−1.4	0.913	0.913	4.34	1.825	1.828	0.040	1
	3-*gas*		0.73	−0.9	0.917	0.917	3.77	1.833	1.836	0.043	
10	**3**-*exp*	B_1-H_{bridge}	0.91(1)	−5.6(1)	0.625	0.713	0.86	1.320	1.345	0.110	2
	4-*exp*		0.93(1)	−5.4(1)	0.619	0.712	0.50	1.320	1.343	0.083	2
	3-*cry*		0.84	−0.5	0.542	0.798	1.44	1.320	1.352	0.113	2
	4-*cry*		0.83	−1.5	0.555	0.796	1.47	1.320	1.358	0.140	2
	3-*gas*		0.85	−2.4	0.566	0.767	1.03	1.317	1.346	0.101	
11	**3**-*exp*	B_3-H_{term}	1.23(3)	−11.2(1)	0.542	0.648	0.01	1.190	1.190	0.006	1
	4-*exp*		1.27(1)	−10.0(1)	0.534	0.656	0.14	1.190	1.190	0.011	1
	3-*cry*		1.17	−5.2	0.510	0.680	0.00	1.190	1.190	0.006	1
	4-*cry*		1.16	−3.4	0.504	0.686	0.01	1.190	1.190	0.006	1
	3-*gas*		1.23	−8.4	0.521	0.663	0.01	1.184	1.184	0.002	

[a] For all bonds, $\rho(\mathbf{r}_{bcp})$ is the ED at the bcp; $\nabla^2\rho(\mathbf{r}_{bcp})$ is the corresponding Laplacian; d_1 and d_2 are the distances from atoms x and y to the bcp; ε is the bond ellipticity [$\varepsilon = (\lambda_1/\lambda_2) - 1; \lambda_1 > \lambda_2$]; R_{xy} is the distance between two bonded atoms; R_{bp} is the length of the topological bond path; Δ_{bcp} is the distance of the bcp position perpendicular to the xy axis; av. is the number of averaged bonds. For all data, see the Supporting Information.

ellipticities larger than what is found in **1**; three have smaller ellipticities.

As is already reflected in the gvf, the difference between R_{xy} and R_{bp} is large for the curved B_0-B_1 bonds (no. 5, about 0.05 Å) and the B_1-H_{bridge} bonds (no. 10, about 0.025 Å) of the *arachno*-boranes. For all other bonds, the values are below 0.015 Å. Accordingly, the same relations are found for Δ_{bcp}. Interestingly, the B_0-B_1 bonds do not have the largest B−B bond ellipticities, which means that strain does not necessarily lead to delocalization. For the strained B_1-H_{bridge} bonds, the situation is different because ϵ is much larger than that for the terminal B−H bonds. In this case, strain and delocalization occur simultaneously.

Topology of rcp's. Table 3 lists the averaged $\rho(\mathbf{r}_{rcp})$ values for the six ring types found in the title compounds. Because the results of models *exp* and *cry* are similar, they were averaged (complete lists of the ring topology are given in the Supporting Information). The $\rho(\mathbf{r}_{rcp})/\rho(\mathbf{r}_{bcp})$ ratio is larger than 0.70 for all B−B bonds, a value much larger than what is known for aromatic or aliphatic C rings. For **1**, $\rho(\mathbf{r}_{rcp})/\rho(\mathbf{r}_{bcp}) = 0.92$ (*exp*); for **2**, $\rho(\mathbf{r}_{rcp})/\rho(\mathbf{r}_{bcp}) = 0.74$ (*exp*, $B_{api}-B_{cen}$) and 0.86 (*exp*, $B_{cenA}-B_{cenB}$). Moreover, ϵ_{rcp} is close to zero for the symmetrical B−B−B deltahedra in **1**, which means that the ED is evenly distributed over the ring plane, whereas the largest value of about 2 is found for the folded four-membered $B_1-H_{bridge}-B_1-B_2$ rings of the *arachno*-boranes. All other rings lie in between. These results confirm the higher degree of delocalization in the deltahedra of **1** compared to the four-membered rings of **2**.

For bond no. 5 (B_0-B_1), which is the long and curved bond in the *arachno*-boranes, the $\rho(\mathbf{r}_{rcp})/\rho(\mathbf{r}_{bcp})$ ratio

Table 3. Averaged Topological Descriptors of rcp's[a]

no.	model	type	$\rho(\mathbf{r}_{rcp})$ [e Å^{-3}]	$\nabla^2\rho(\mathbf{r}_{rcp})$ [e Å^{-5}]	$d_{av.}$ [Å]	λ_1 [e Å^{-5}]	ϵ_{rcp}	av.	type
a	**1**-*exp*/*cry*	B−B−B	0.73	−0.4	1.032	−3.29	0.09	20	3
	1-*gas*		0.72	0.1	1.030	−3.13	0.01		
b	**2**-*exp*/*cry*	$B_{cenA}-B_{cenB}-B_{cenA}-B_{api}$	0.66	0.0	1.055	−2.91	0.64	8	4
	2-*gas*		0.65	0.5	1.056	−2.71	0.53		
c	**3**-*exp*/*cry*	$B_0-B_2-B_1$	0.78	−1.0	1.032	−3.66	0.56	12	3
	3-*gas*		0.75	−0.4	1.028	−3.40	0.21		
d	**3**-*exp*/*cry*	$B_1-B_2-B_3$	0.78	−0.5	1.019	−3.49	0.43	8	3
	3-*gas*		0.75	−0.1	1.017	−3.27	0.49		
e	**3**-*exp*/*cry*	$B_3-B_2-B_3$	0.73	−0.3	1.036	−3.29	1.14	6	3
	3-*gas*		0.72	0.1	1.032	−3.08	0.90		
f	**3**-*exp*/*cry*	$B_1-B_3-B_1-H_{bridge}$	0.68	0.4	1.058	−3.04	1.99	4	4
	3-*gas*		0.65	0.7	1.057	−2.76	1.92		

[a] For all bonds, $\rho(\mathbf{r}_{rcp})$ is the ED at the rcp; $\nabla^2\rho(\mathbf{r}_{rcp})$ is the corresponding Laplacian; $d_{av.}$ is the averaged distance of the three closest ring atoms to the rcp; λ_1 is the curvature of the ED perpendicular to the ring plane; ϵ_{rcp} is the ring plane ellipticity [$\epsilon_{rcp} = (\lambda_2/\lambda_3) - 1; \lambda_2 > \lambda_3$]; av. is the number of averaged rings; type is the ring type (three- or four-membered).

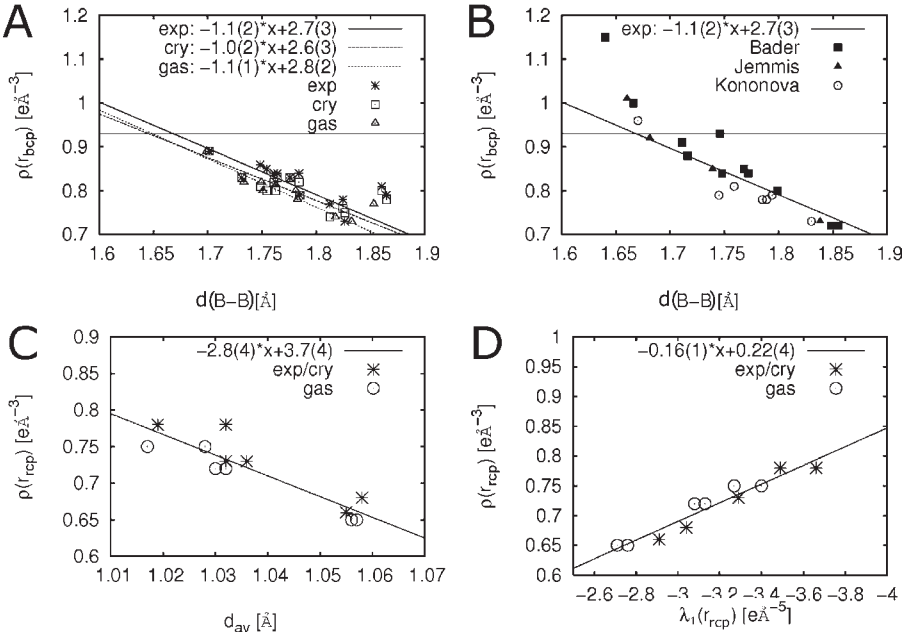

Figure 5. (A) ED value at the bcp vs B−B bond length: experimental results (*exp*) and calculations under periodic boundary conditions (*cry*) and of the optimized gas-phase structures (*gas*). (B) Calculated values of refs 42, 44, and57 in relation to the best-fit line obtained for *exp*. (C) ED at the rcp vs averaged distances of the atoms to the rcp. (D) ED at the bcp vs λ_1. The horizontal lines in parts A and B correspond to the $\rho(r_{rcp})$ value defined by Bader and Legare[42] as being of bond order 1.0.

increases to 0.99 (*exp*), but in this case, the ratio does not reflect delocalization because the bcp is extremely close to the rcp (see Figure 3C) and the absolute $\rho(\mathbf{r}_{bcp})$ value of that bond is smaller than that for the other two bonds of that ring.

Relationships between Geometry and Topology. Some properties at bcp and rcp show linear relationships to geometrical B−B (B−rcp) distances. Figure 5A displays the averaged $\rho(\mathbf{r}_{bcp})$ values plotted against the averaged B−B distances, as listed in Table 2 for models *exp*, *cry*, and *gas*. In Figure 5B, the corresponding plot is given for theoretically obtained $\rho(\mathbf{r}_{bcp})$ values of diverse borane structures from refs 42, 44, and 57. Also, for $\rho(\mathbf{r}_{rcp})$, a relationship is found for the averaged distances of the three closest ring atoms; see Figure 5C. Finally, in Figure 5D, $\rho(\mathbf{r}_{rcp})$ is plotted against λ_1(rcp). The horizontal line in Figure 5A,B corresponds to $\rho(\mathbf{r}_{bcp}) = 0.93$ e Å^{-3} calculated for the B−B bond in the *arachno*-borane B_4H_{10} by Bader and Legare.[42] Because this is the smallest known borane structure exhibiting a (single) B−B bond, they defined this bond as being of bond order 1.0. According to this, all observed/calculated B−B bonds in Figure 5A have a bond order smaller than 1.0, as is common for boranes.

The lines of best fit in Figure 5A were calculated under exclusion of the strained B_0-B_1 bond of the *arachno*-boranes because this bond type obviously does not follow the proposed linear relationship. The slopes of the best-fit lines obtained for the different models are comparable, although the statistical basis is quite small. The experimental line (solid) is positioned above the density functional theory (DFT) calculations (dotted) as was also found for an ED analysis of a large variety of C−C bonds in substituted fullerenes.[15] In Figure 5B, the best-fit line of the experimental results (*exp*) obtained for Figure 5A is also plotted. One finds a good agreement with the results from the literature. The two exceptions are the central B−B bond in the *nido*-borane B_6H_{10} and the

Table 4. Integrated Bond Descriptors for the Isolated Compounds at Optimized Geometries, Model *gas*[a]

compd	type	$\delta(x,y)$	ELI_{pop} [e]	V_{001}^{ELI} [Å^3]	ELI_{max} γ	Δ_{ELI} [Å]	SF_x [e Å^{-3}] (%)	SF_y [e Å^{-3}] (%)	SF_{x+y} [e Å^{-3}] (%)
1	B−B	0.48	0.81	1.9	1.52	0.105	0.19 (23.9)	0.18 (23.6)	0.37 (47.5)
2	$B_{api}-B_{cen}$	0.59	1.17	3.4	1.55	0.170	0.24 (26.9)	0.25 (28.0)	0.49 (54.9)
	$B_{cenA}-B_{cenB}$	0.48	0.92	2.3	1.52	0.090	0.17 (22.5)	0.18 (23.8)	0.34 (46.3)
	$B_{cenA}-B_{cenA}$	0.41	0.47	1.3	1.47	0.329	0.14 (19.7)[b]	0.14 (19.7)[b]	0.28 (39.4)[b]
3	B_0-B_1	0.48	1.86	5.0	1.78	0.134	0.19 (25.2)	0.18 (23.5)	0.37 (48.7)
	B_0-B_2	0.46					0.21 (26.2)	0.19 (23.4)	0.40 (49.6)
	B_1-B_2	0.45					0.19 (23.7)	0.19 (23.2)	0.38 (46.9)
	B_1-B_3	0.46	1.39	3.2	1.56	0.137	0.18 (22.9)	0.20 (24.5)	0.38 (47.4)
	B_2-B_3	0.48	0.86	1.9	1.53	0.091	0.21 (25.0)	0.20 (24.9)	0.41 (49.9)
	B_3-B_3	0.38	0.53	1.1	1.47	0.080	0.15 (20.7)	0.15 (20.7)	0.30 (41.4)
1	B−H	0.71	2.06	15.5	8.24		0.37 (32.2)	0.55 (47.0)	0.92 (79.2)
2	$B_{api}-H$	0.73	2.09	16.8	7.88		0.38 (33.4)	0.58 (51.0)	0.96 (84.4)
	$B_{cen}-H$	0.71	2.06	15.8	7.90		0.37 (32.3)	0.52 (45.8)	0.89 (78.1)
3	B_0-H_0	0.64	1.99	12.2	7.40		0.42 (34.0)	0.58 (47.9)	1.00 (81.9)
	B_1-H_1	0.69	2.02	14.8	8.24		0.41 (33.9)	0.60 (49.6)	1.01 (83.5)
	B_2-H_2	0.69	1.99	13.3	8.29		0.39 (32.9)	0.60 (50.7)	0.99 (83.6)
	B_3-H_3	0.73	2.02	14.5	8.44		0.42 (34.4)	0.62 (50.5)	1.04 (84.9)
	B_1-H_{bridge}	0.43	1.96	7.6	4.84		0.23 (26.7)	0.28 (32.8)	0.51 (59.5)

[a] For all bonds, $\delta(x,y)$ is the delocalization index of atoms x and y; ELI-D_{pop} is the electron population of the ELI-D basins; V_{001}^{ELI} is the corresponding volume cut at an ED value of 0.001 au; ELI_{max} is the corresponding ELI-D value at the attractor position; Δ_{ELI} is the distance of the attractor position perpendicular to the xy axis; SF_x [e Å^{-3}] and SF_y [e Å^{-3}] are the integrated source contributions of the direct bond partners; SF_{x+y} [e Å^{-3}] is the sum of both contributions. [b] The midpoint of the $B_{cenA}-B_{cenA}$ axis was chosen as the rp for calculation of the SF.

above-mentioned B−B bond of the *arachno*-borane B_4H_{10}, which show a significantly larger $\rho(\mathbf{r}_{bcp})$ than the delocalized B−B bonds close to the experimental best-fit line.[87] These bonds are significantly more localized because the possibility of delocalization is dependent on the number of adjacent B−B−B deltahedra or, in other words, on the location of the B−B−B triangle within the molecular structure.

Figure 5C shows the averaged distances of the ring atoms to the rcp ($d_{av.}$) plotted against $\rho(\mathbf{r}_{rcp})$. All data (*exp*/*cry* and *gas*) were used in this case for the fit to enlarge the statistical base. Interestingly, λ_1 shows the very same behavior as $\rho(\mathbf{r}_{rcp})$; see Figure 5D.

Considering these observations, one may state that, although many different B−B bond types and B−B−B (B−B−B−B and B−H−B−B) ring types are present in the four title compounds with different degrees of delocalization and strain, geometry and ED are still related to each other in a quite simple fashion. The delocalized bonds can clearly be distinguished from the localized bonds by the behavior of the ED at the bcp position but not unambiguously by the bond ellipticities, the difference between R_{bp} and R_{xy}, or the Δ_{bcp} values.

Integrated Bond Descriptors. In addition to the canonical topological bond properties, integrated descriptors like the ELI-D and SF are analyzed in order to shed more light on the nature of the 2e3c bonds of deltahedral boranes; see Table 4 for the model *gas*.

For the ELI-D, the electron populations within the valence basins (ELI_{pop}) are given together with the corresponding volumes (V_{001}^{ELI}), which were cut at 0.001 au of the ED, the values of the ELI-D attractors (ELI_{max}), and, finally, the distance of the attractors perpendicular to the B−B or B−H axis (Δ_{ELI}). Moreover, the integrated absolute and relative source contributions of neighboring B atoms (SF_x and SF_y) are given, which were summed up to SF_{x+y}.[88] For the ELI-D and SF, complete lists are given in the Supporting Information.

Generally, $\delta(x,y)$ and ELI_{max} are small in boranes but much larger for the localized B−H bonds than for the B−B bonds, with the exception of the strained and delocalized $B-H_{bridge}$ bond, for which both are small as well. No relation of $\delta(x,y)$ and the bond lengths could be detected. The SF is inconclusive, which may be related to the recent criticisms made by Farrugia and Macchi concerning the interpretation of the SF in delocalized systems.[89]

Interestingly, in the *arachno*-boranes, two types of adjacent B atoms that have a bcp in the AIM scheme do not have an ELI-D basin (B_0-B_2 and B_1-B_2). On the other hand, an ELI-D basin is found for $B_{cenA}-B_{cenA}$, which does not have a bcp.[90] However, for both types of pairs, δ(B,B) is on the same order of magnitude as that for the other pairs. The results of this work confirm that the absence of a bcp does not necessarily indicate the absence of chemical bonding because significant electron sharing is found in terms of $\delta(x,y)$ and the ELI-D. We note that the three questions about the influence of the geometry changes, the computational method, and the ambiguities/restrictions of the multipole model itself that were given in the introduction were not investigated in this work because they were beyond possibility and scope, but all points require further effort.

When δ(B,B) is averaged, the values are almost identical for the two *closo*-boranes (about 0.48) but smaller for the *arachno*-boranes (about 0.43). In contrast, the

(87) The data of Bader and Legare (black squares[42]) and of Jemmis et al. (black triangles[44]) are based on Hartree−Fock calculations and lie above the DFT results of Kononova et al. (white circles[57]). This was also found in the above-mentioned study on fullerenes.[15]

(88) For all listed properties, small differences are found between **4** and **3**, but because the SF could only be obtained for **3**, only this compound is included here.

(89) Farrugia, L. J.; Macchi, P. *J. Phys. Chem. A* **2009**, *113*, 10058–10067. For definition and application of the SF, see refs 33 and 34.

(90) In order to reveal if the different bonding patterns of ELI-D compared to AIM are an artificial result of the grid size or if they reflect the bonding pattern truly, the calculations were repeated for **2** and **3** with a grid size of 0.05 au (newest upload of *DGRID-4.5*). All topological features of the *DGRID-4.4* calculations were confirmed. The corresponding ELI-D populations are given in the Supporting Information.

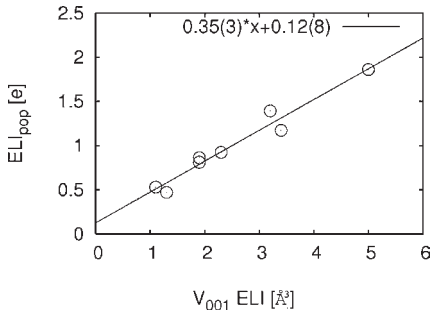

Figure 6. Electron populations vs corresponding volumes of the ELI-D basins of the four geometry-optimized models in the gas phase. Both volumes and populations are cut at an ED value of 0.001 au.

populations of the B−B bonding basins show the opposite behavior. The highest averaged populations of about 1.31 e are found for the *arachno*-boranes. For **1** and **2**, the values are 0.81 and 0.85 e. Although the ELI_{pop} values and the volumes of the basins[91] vary considerably, a nearly perfect linear relationship is found between ELI_{pop} and $V_{001}{}^{ELI}$. Figure 6 displays this relationship. Because three different structure types are included in this analysis, the assumption might be justified that this is a general feature of the ELI-D in boranes. As one would expect, the axis intercept is very close to zero in the best-fit line.

The "missing" $B_{cenA}-B_{cenA}$ bonding in compound **2** and the strained but "localized" bond in the *arachno*-boranes (B_0-B_1) again are the borderline cases with respect to δ(B,B) and the ELI-D. For $B_{cenA}-B_{cenA}$, the values of δ(B,B), ELI_{pop} (and, thus, $V_{001}{}^{ELI}$), and ELI_{max} are much smaller than those for $B_{cenA}-B_{cenB}$ or $B_{api}-B_{cen}$. Furthermore, the distance of the ELI-D maximum perpendicular to the B−B axis is as large as 0.329 Å, which also points toward a very weak connection and may explain the missing bcp. With the exception of Δ_{ELI}, all integrated bond discriminators of $B_{cenA}-B_{cenA}$ are close to those of B_3-B_3 in the *arachno*-boranes. For the latter pair of B atoms, a bcp is found, but the ED at this point is smaller than that for the other B−B bonds and the ellipticity is higher.

In contrast, B_0-B_1 shows the largest ELI_{pop}, $V_{001}{}^{ELI}$, and ELI_{max} values of all B−B bonds in this work. δ(B,B) is large as well, and Δ_{ELI} is much smaller than that for $B_{cenA}-B_{cenA}$. For B_1-B_1, neither an AIM-bcp nor an ELI-D basin is found. $\delta(B_1,B_1) = 0.20$ in compounds **3** and **4**. The integrated source contributions of the B_1 atoms are as small as 12.5%, whereas the bridging H atom contributes 26.7%. Considering the results, only $\delta(x,y)$ corresponds to some extent to the expected bonding pattern in the investigated deltahedral boranes; the absence of an AIM-bcp and/or ELI-D disynaptic valence basin does not provide an unambiguous criterion for the absence of a bonding interaction.

Figures 7 and 8 display the shapes of the ELI-D localization domains of the four title compounds, each at $\gamma = 1.3$ and at an individually chosen higher value to make the positions of the ELI-D maxima visible. At $\gamma = 1.3$, all compounds show the expected polyhedra dual to the boron cages. For the corresponding images at individual values, γ was varied in the small range of 1.47−1.50. In all cases, the maxima are located outside the boron cages. In **1**, all localization domains are of equal shape because of the high molecular symmetry. For **2**, a ringlike arrangement of the localization domains is visible because the $V_2(B_{cen},B_{cen})$ domains point toward each other, as do the $V_2(B_{cen},B_{api})$ domains. In view of this, the general picture of a localization function evenly covering the deltahedral surfaces is misleading because the different ELI-D basins are not comparable in size or population nor do they correspond to the molecular scheme generated by AIM topology.

Conclusion

In borane chemistry, no single necessary criterion for "chemical bonding" has been deduced up to now from real-space functions such as the ED or a localization function.

The highly symmetrical compound **1** exhibits bcp's between all 30 pairs of B atoms and corresponding rcp's of nearly the same ED values for both critical bond types, which reflects the high degree of delocalization of the electrons. This is supported by high B−B bond ellipticities. Also, in the ELI-D scheme, a disynaptic B−B bond basin is found between all pairs of B atoms. The attractors are located outside the borane cage close to the B−B axis and not in the center of the B−B−B triangles, as one might assume because the localization functions have the shape of the polyhedron dual to the icosahedron (which is the dodecahedron).

For AIM and ELI-D analysis of the less symmetric compounds **2**−**4**, ambiguous results are found considering the molecular graph (or chemical structure). In **2**, no bcp is found between B_{cenA} and B_{cenA}, whereas a disynaptic ELI-D basin is located between these atoms. The volume and electronic population is weak for this basin type, but the delocalization index $\delta(B_{cenA},B_{cenA})$ is on the same order of magnitude as that for the other B−B interactions.

In the *arachno*-boranes, the bonding situation shows features opposite to those of $B_{10}H_{10}{}^{2-}$. For B_0-B_2 and B_1-B_2, no ELI-D basins are found, although bcp's are located between the atoms. Again, the delocalization index is on the same order of magnitude as that for the other bonds. For B_1-B_1, no bonding interaction is detected in terms of AIM and ELI-D, thus leading to a folded four-membered ring $B_1-H_{bridge}-B_1-B_3$ with AIM topology comparable to the four-membered ring in compound **2**. Nevertheless, $\delta(B_1, B_1)$ is not close to zero but has a value of 30−50% of that of the other pairs of adjacent B atoms.

Although the bonding patterns are quite different in the three general structure types icosahedron, bicapped square antiprism, and *arachno*-cage, simple relationships were, nevertheless, found between B−B bond distances (B−B−B ring sizes) and topological parameters; this is known for conventional organic compounds but has not yet been examined for boranes. Moreover, the plot of $V_{001}{}^{ELI}$ versus ELI_{pop} shows an almost perfect linear relationship.

The B_0-B_1 bond shows a behavior that is different from that of all other B−B bonds. It is the longest B−B bond in the four title complexes, with a bond path being extremely curved inward the B−B−B ring. The bond ellipticity is, nevertheless,

(91) Because orbitals are diffuse but the ELI-D partitioning is sharp, the populations of the ELI-D basins are never found to be in integer numbers.

(92) Hübschle, C. B.; Luger, P. Moliso—a program for colour-mapped iso-surfaces. *J. Appl. Crystallogr.* **2006**, *39*, 901−904.

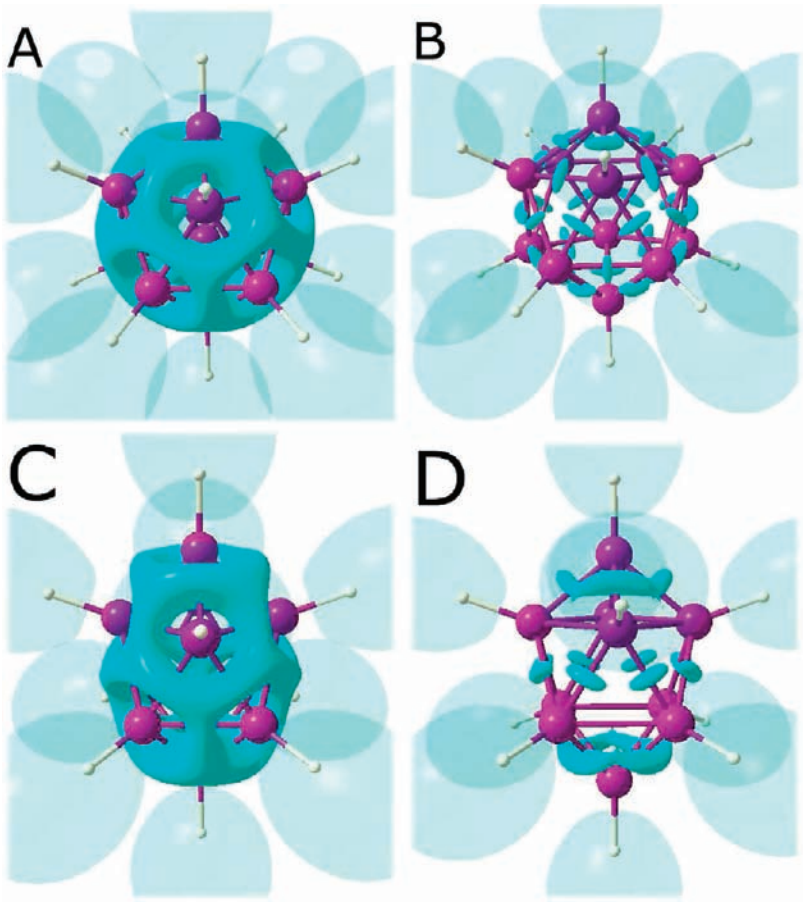

Figure 7. Localization domains of the ELI-D for compounds **1** and **2**: (A) $\gamma = 1.30$; (B) $\gamma = 1.48$; (C) $\gamma = 1.30$; (D) $\gamma = 1.47$. Hydrogen domains are given in transparent mode. Moliso representation.[92]

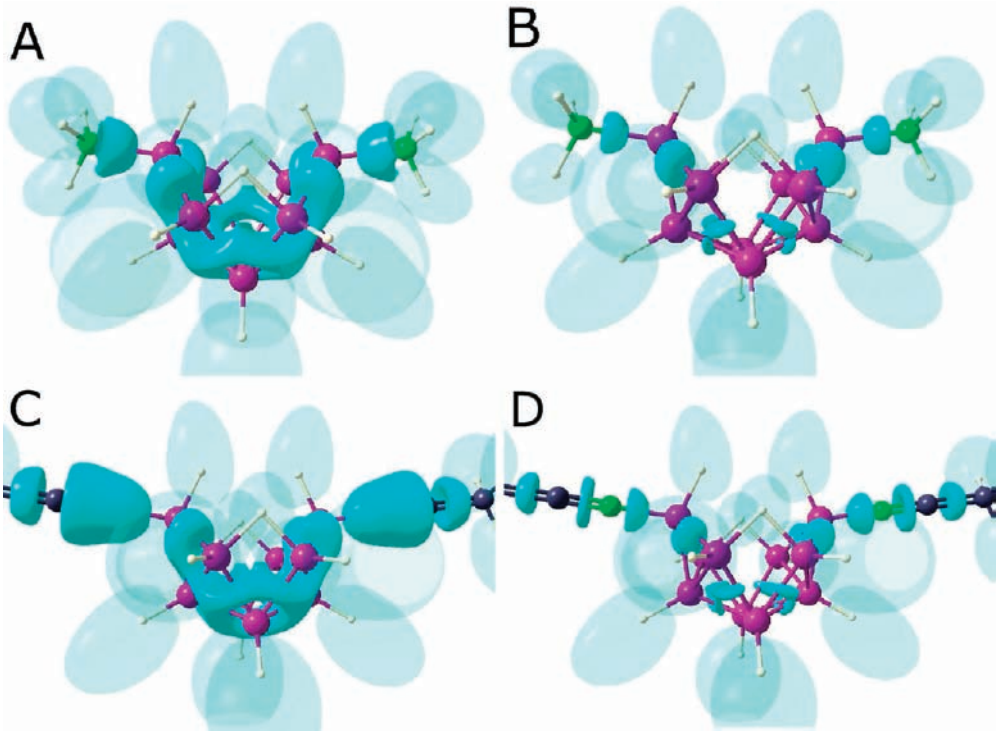

Figure 8. Localization domains of the ELI-D for compounds **3** and **4**: (A) $\gamma = 1.30$; (B) $\gamma = 1.50$; (C) $\gamma = 1.30$; (D) $\gamma = 1.50$. Hydrogen domains are given in transparent mode. Moliso representation.[92]

smaller in comparison to most other B−B bonds, and the delocalization index is quite high, considering the long B−B distance of this bond. Furthermore, an ELI-D basin is found for this bond but not for the adjacent pairs B_0-B_2 and B_1-B_2, and ELI_{max} is significantly larger than that for all other B−B bonds in compounds **1**−**4**. Finally, $\rho(\mathbf{r}_{bcp})$ does not follow the linear relationship of d(B−B) versus $\rho(\mathbf{r}_{bcp})$, which is found for all other B−B bonds because it is much larger at the B_0-B_1 bcp. Examples of other localized and delocalized B−B bonds were found in the literature, which confirms the results of this study.

The $B-H_{bridge}$ bond, on the other hand, is also longer and more strained than all other B−H bonds. For this bond, however, all bond topological and integrated properties point toward a higher degree of delocalization than that for the terminal B−H bonds.

Acknowledgment. We thank the Deutsche Forschungsgemeinschaft (DFG Grants LE423/13-3 and LU222/30-2 within SPP1178) for financial support. Miroslav Kohout and Julian Henn are thanked for helpful discussions. Christian Hübschle is thanked for his help with the ELI-D images.

Supporting Information Available: CIF files of protonated lutidinium dodecahydro-*closo*-dodecaborate(2−), monoprotonated 2,2′-bispyridilium decahydro-*closo*-decaborate(2−), dodecahydro-*arachno*-bis-amin borane, and dodecahydro-*arachno*-bis-acetonitrile borane (CCDC 779590, CCDC 779589, CSD 421863, and CCDC 779588), details of data processing, details of wave-function analysis, complete geometries and topologies of models *exp*, *cry*, and *gas* including labeling schemes, packing diagrams of the four compounds along crystallographic axes, experimental sdd maps, corresponding Laplacian and gvf maps of three rings of compound **3**, experimental ED line plots for B−B in **1** and B_1-B_1 in **3**, theoretical ED line plots for **2**, experimental ED line plots through the molecules **1** and **2**, complete SF contributions and ELI-D parameters (populations, volumes, and attractor values) of the four gas-phase calculations, and complete ref 75. This material is available free of charge via the Internet at http://pubs.acs.org.